LETTERS

Phase-resolved measurements of stimulated emission in a laser

Josef Kröll[1], Juraj Darmo[1], Sukhdeep S. Dhillon[2,3], Xavier Marcadet[4], Michel Calligaro[4], Carlo Sirtori[2] & Karl Unterrainer[1]

Lasers are usually described by their output frequency and intensity. However, laser operation is an inherently nonlinear process. Knowledge about the dynamic behaviour of lasers is thus of great importance for detailed understanding of laser operation and for improvement in performance for applications. Of particular interest is the time domain within the coherence time of the optical transition. This time is determined by the oscillation period of the laser radiation and thus is very short. Rigorous quantum mechanical models[1,2] predict interesting effects like quantum beats, lasing without inversion, and photon echo processes. As these models are based on quantum coherence and interference, knowledge of the phase within the optical cycle is of particular interest. Laser radiation has so far been measured using intensity detectors, which are sensitive to the square of the electric field. Therefore information about the sign and phase of the laser radiation is lost. Here we use an electro-optic detection scheme to measure the amplitude and phase of stimulated radiation, and correlate this radiation directly with an input probing pulse. We have applied this technique to semiconductor quantum cascade lasers, which are coherent sources operating at frequencies between the optical ($>$100 THz) and electronic ($<$0.5 THz) ranges[3]. In addition to the phase information, we can also determine the spectral gain, the bias dependence of this gain, and obtain an insight into the evolution of the laser field.

Since the realization of the first laser, researchers have investigated stimulated emission and the gain in an amplifying medium using coherent or incoherent radiation[1]. Several well known phenomena have been observed in these very basic experiments—spectral narrowing, power broadening, gain saturation, and the spectral gain curve[4–7]. With the advent of ultrashort laser pulses, time-resolved spectroscopy with a time resolution better than 10 fs has become possible[8]. At the same time, femtosecond-laser-driven generation of few-cycle phase-locked terahertz (THz) pulses has paved the way towards coherent detection of transient THz electric fields using electro-optic sampling[9]. This latest generation of phase-resolved femtosecond spectroscopy has recently enabled the observation of the birth of the plasmon-phonon mode[10] and of excitons in semiconductors[11], as well as the observation of gain associated with an optically pumped excitonic system in Cu_2O (ref. 12).

The phase-resolved measurement of stimulated emission in lasers has however still been hindered by the rather fast electric field oscillations in conventional lasers (about 2.5 fs at 800 nm). The situation has changed dramatically with the realization of THz quantum cascade lasers (THz-QCL) emitting in a wide frequency range from 4.4 THz down to 1.6 THz (refs 13, 14). Accordingly, the time resolution required to resolve the electric field oscillations of the THz-QCL emission has been brought down to several tens of femtoseconds, which is readily accessible by modern femtosecond spectroscopy.

With the set-up described in the Methods section we have direct access to the amplitude and phase of the THz pulses transmitted through the laser. Knowledge of the phase is essential when studying optical processes in an inverted system. From the quantum mechanical description of stimulated emission, it is known that incoming photons generate a superposition between ground state and first excited state. This superposition constitutes an oscillating dipole that emits electromagnetic waves. The difference between amplification and attenuation is solely determined by the phase of this superposition. When the incoming and the dipole fields are in-phase, constructive interference and amplification will be observed. Destructive interference and thus attenuation of the transmitted pulse will be observed when these fields are out-of-phase. In the present detection scheme, we resolve the phase of the superposition directly from the relative phase between probe and emitted electric fields.

The pulse transmitted through the unbiased THz-QCL (Fig. 1a) resembles the input pulse followed by small oscillations, which point to a weak absorption in the THz-QCL waveguide. When the laser is biased, the shape of the differential transmission of the THz pulse changes significantly (Fig. 1b). The time domain signal is now a result of changed absorption and gain in the biased THz-QCL. The transient THz field is dominated by a very pronounced oscillation lasting several picoseconds. These oscillations are due to stimulated emission and thus amplification of the incident pulse. It can be seen that there is a phase jump between the oscillating part and the initial pulse, as indicated by an arrow in Fig. 1b. In Fig. 1c we compare these data to a finite-difference time-domain simulation of the pulse propagation in the two-level system[15,16] described in Methods and Supplementary Information. We find excellent agreement with respect to the envelope and phase of the oscillations if we assume a population inverted system with a gaussian distribution of the resonant frequencies centred at 2.9 THz, a coherence time T_2 of 7 ps, and a non-radiative decay time of 1.5 ps.

From the discrete Fourier transformation of the modulation signal, we obtain the absorption spectrum and phase (Fig. 2a and b, respectively). The absorption is dominated by a negative peak at about 2.9 THz, representing the spectral gain of the THz-QCL. The frequency dependence of the phase—displaying the negative part on the low-frequency side of the resonance—is inverted compared to the usual behaviour for resonant absorption. This behaviour is the unambiguous evidence for gain and thus population inversion. With knowledge of the phase, we can distinguish between amplification and loss. Thus we can attribute the broadband positive feature at frequencies between 1.0 and 2.2 THz to increased loss in

[1]Photonics Institute, Vienna University of Technology, Gusshausstrasse 25-29, A-1040 Vienna, Austria. [2]Matériaux et Phénomènes Quantiques, Université Paris 7, 75251 Paris Cedex 05, France. [3]Ecole Normale Superieure, 75231 Paris Cedex 05, France. [4]Alcatel-Thales III-V Lab, Route Départementale 128, 91767 Palaiseau Cedex, France.

the THz-QCL caused by differences in the carrier distribution in the unbiased and biased active region. This broadband absorption causes the initial pulse of the THz transient in Fig. 1b. In Fig. 2c, the spectral gain is shown for different bias current densities. Below threshold, we observe an almost gaussian gain profile with a bandwidth (full-width at half-maximum) of about 130 GHz. Above threshold (at 165 A cm^{-2}), the gain curve is changed and we observe a dip in the gain spectrum. We explain this by gain clamping at the frequency of the Fabry–Perot cavity mode. The position of this hole coincides exactly with the Fabry–Perot mode at 2.87 THz of the lasing QCL, which was measured separately using a Fourier transform infrared spectrometer. The observation of the dip in the spectral gain is possible because the THz-QCL is working in a single mode condition (for a discussion of the interaction between a laser field and the spatial distribution of gain, see ref. 17). Note that we are observing the gain spectrum while the laser is above threshold. This measurement is unique, and illustrates the enormous potential of our technique.

The potential of electro-optic sampling is further demonstrated by looking at the pulses that are reflected at the facets of the Fabry–Perot resonator of the QCL. These reflected pulses are temporally separated by the cavity round-trip time. We perform these measurements below threshold at a current density of 110 A cm^{-2} to avoid the above-mentioned effects of spatial gain modulation in the QCL lasing at the Fabry–Perot modes. This would cause a more complex evolution of the multiple reflected pulses. Staying below threshold provides a homogeneous gain and allows a straightforward explanation of the results. Figure 3 displays pulses after a few passes through the cavity. The amplitude of the pulse after three passes (Fig. 3b) is comparable to that of the direct transmission (Fig. 3a), but the pulse duration is significantly extended. The initial feature corresponding to the broadband response of the incident pulse is completely gone. After five passes (Fig. 3c), the amplitude of the oscillation appears to be lower, the duration of the pulse is again longer and the total energy in the pulse is slightly less than that of the three-pass pulse. The observed pulse duration tendency points to the spectral narrowing of the pulses. The energy carried by the individual pulses decreases because the total propagation losses prevail over gain when the laser is driven below threshold.

Finally, we focus on the bias current dependence of the single-pass gain and correlate it with the light output and the current–voltage characteristics (Fig. 4). This comparison reveals details about the internal processes in the active region of the QCL. Without applied bias or with low bias, the THz-QCL exhibits no resonant absorption at the lasing frequency (~2.9 THz) usually expected for an unpumped gain medium. However, without the correctly applied bias the energy levels in the QCL are not properly aligned[18], thus the designed optical transition cannot occur and no resonant absorption can be observed. A measurable gain appears only when most of the cascades in the active region are properly aligned, which is indicated by a change in the differential resistance at a bias of ~ 2.1 V (Fig. 4c). After the onset, the gain rises proportionally with bias current density owing to an increasing population inversion. The lasing threshold is reached at a bias current density of about 113 A cm^{-2}, where we obtain a single-pass gain of ~19 cm^{-1}. This value compares to calculated waveguide losses of 7–11 cm^{-1} (refs 19–21) and to a value of 12 ± 1 cm^{-1} obtained from measurements of unbiased THz-QCL waveguides at different lengths. We assume

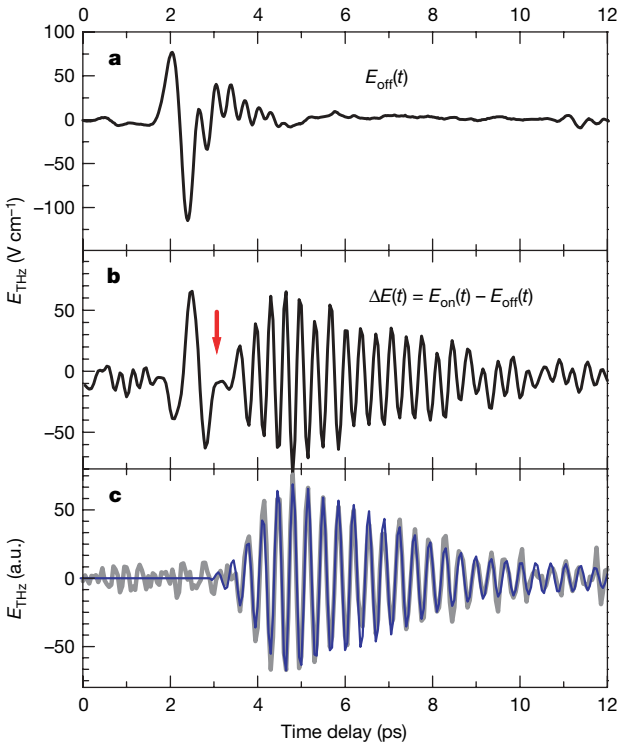

Figure 1 | Terahertz time-domain spectroscopy of a THz-QCL. **a**, The electric field waveform, $E_{off}(t)$, of a THz pulse transmitted through an unbiased THz-QCL. **b**, Change in the transmitted pulse waveform, $\Delta E(t)$, induced by biasing the THz-QCL. The signal is dominated by strong oscillations. A phase jump occurs between the initial pulse and the oscillations indicated by an arrow. **c**, Comparison of a simulation (thin blue line) to $\Delta E(t)$ spectrally filtered by a band-pass filter 2.0–3.5 THz (grey line). The leading part of the terahertz pulse disappears because it carries only broad-band low frequency components below 2 THz. The bias current density was 110 A cm^{-2}.

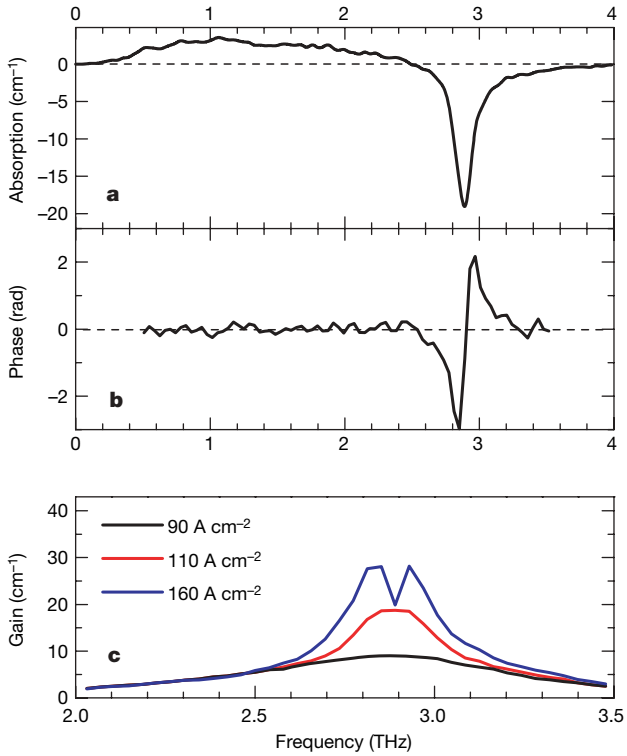

Figure 2 | Fourier transform of the transmission signal modulated by the THz-QCL. **a**, The absorption shows a negative part (gain) and positive part (reduced transmission). **b**, The phase change retrieved from the THz electric field shows an inverted dispersive behaviour, as expected from an inverted system. **c**, Spectral gain of the THz-QCL driven at 90, 110 and 160 A cm^{-2}. For the highest bias current density, the device is lasing at a single Fabry–Perot mode. We observe a dip in the spectral gain corresponding to the frequency of the Fabry–Perot mode. For this frequency, the gain is clamped at the threshold value.

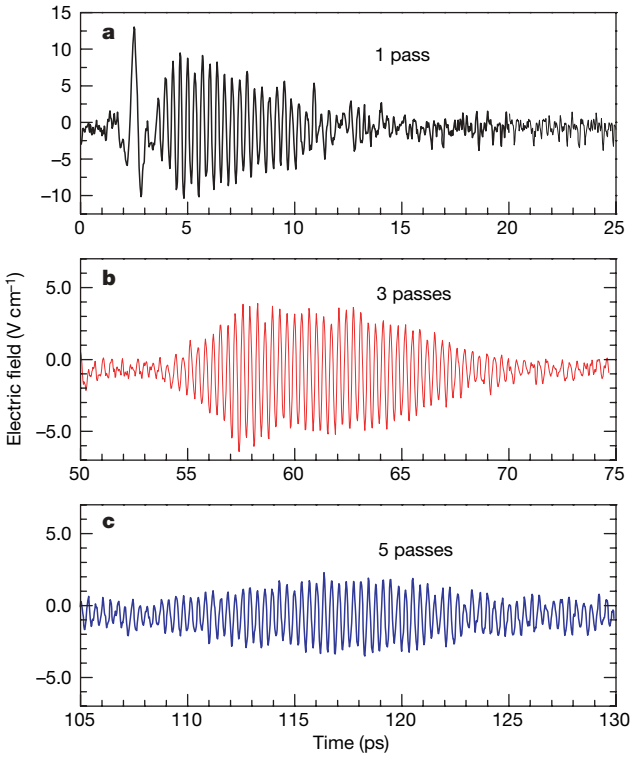

Figure 3 | Build-up of the electric field oscillations phase-locked to the external source. **a**, Waveform of the directly transmitted (single pass) THz pulse. **b**, The pulse waveform after three passes through the cavity. The pulse amplitude is comparable to that of the direct transmission, but the duration is significantly extended and the initial part of the pulse has vanished. **c**, After five passes, the amplitude of the oscillation appears to be lower, but the pulse length is now much higher—the total energy in the pulse is almost the same as for the three-pass pulse. The THz-QCL is operated slightly below threshold at a current density of 110 A cm^{-2}. The pulses are temporally separated by the cavity round-trip time.

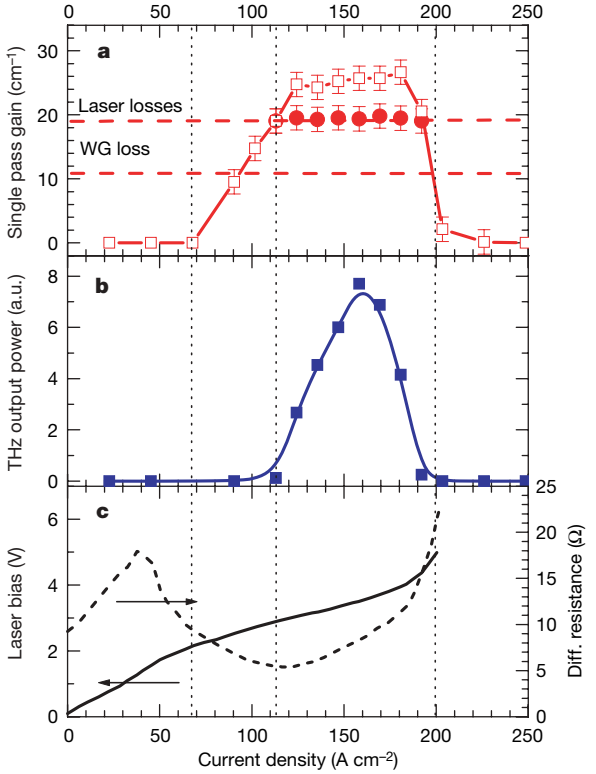

Figure 4 | Bias current characteristics of the THz QCL. **a**, Single-pass gain obtained from the electro-optic measurement at the spectral hole (2.87 THz, filled symbols) corresponding to the saturated gain, and evaluated at the maximum of the spectral gain (2.95 THz, open symbols) representing the unsaturated gain. WG, waveguide. Error bars indicate standard deviation. **b**, Average output power of the QCL measured by a photo-acoustic detector, showing the threshold and the dynamic range. **c**, Current–voltage curve (solid line) and differential resistance (dashed line) of the QCL. The QCL is operated in pulsed mode at a repetition rate of 17 kHz and a duty cycle of 15%.

mirror losses as high as 7 cm^{-1} because of a silicon hemispherical coupling lens attached to one waveguide facet.

The bias current dependence of the single-pass gain changes significantly when the lasing threshold is reached, which is detected by a sudden increase of the total THz output intensity recorded by the intensity detector (a Golay cell; Fig. 4b). The single-pass gain of the THz pulse, however, does not increase linearly any more in this current range, but it becomes almost 'clamped' at the threshold value. The standing-wave pattern of the laser mode leads to a local gain clamping at the antinodes, while the gain remains unclamped at the nodes. The THz pulse passing through the laser cavity probes both saturated and unsaturated gain areas, resulting in the apparent hole in the gain spectrum (Fig. 2c). We can therefore determine the unsaturated and clamped gain values (Fig. 4a).

In contrast to diode lasers, the gain of the THz-QCL is maintained for a limited dynamical range (Fig. 4a). This is explained by a gradual decrease of the injection into the upper lasing level due to field-induced shifts of the injector levels[18]. Associated with this effect is a clearly observable steep increase of the QCL's differential resistance above bias current densities >180 A cm^{-2} (Fig. 4c).

With phase-resolved measurements of the gain in laser media, a whole class of new experiments can be performed and fundamental physical parameters accessed. By noting the sign of the phase, it is possible to unambiguously determine gain or loss. Using both electro-optic field detection and intensity measurements provides the basis for making simultaneous observations of amplification and self-sustained lasing. Access to these separate processes allows the study of waveguide or other optical losses, as well as the examination of nonlinear effects like saturation, gain clamping, and spatial hole burning. The technique we have presented is not limited to QCLs, but is applicable to any gain medium. With the recent development of phase-locked extreme-ultraviolet pulse generation, the electric field on the attosecond timescale can be resolved[22], allowing the technique we have presented here to be used in the infrared and visible spectral range.

METHODS SUMMARY

We use THz time-domain spectroscopy[23] to access the coherent temporal properties of the THz-QCL. Quasi-single-cycle THz pulses, generated by exciting a photoconductive switch[24] with 80-fs-long, infrared laser pulses from a Ti:sapphire laser, are transmitted through the THz-QCL waveguide. Coherent electro-optic detection[9] is used to sense the instantaneous electric field vector of the transmitted THz pulses. Complementary to the electro-optic detection we use also a photo-acoustic detector (a Golay cell). This detector registers the total THz intensity emitted from the laser, while the electro-optic detector is sensitive only to the THz radiation which is phase-locked with respect to the incident THz pulse. The measurements are performed on an AlGaAs/GaAs THz-QCL with a bound-to-continuum optical transition designed for 2.9 THz (refs 19, 20). Details of the experimental technique and the design of the THz-QCL are given in Methods and Supplementary Information.

Full Methods and any associated references are available in the online version of the paper at www.nature.com/nature.

Received 16 March; accepted 20 August 2007.

1. Scully, M. O. & Lamb, W. E. Quantum theory of an optical maser. I. General theory. *Phys. Rev.* **159**, 208–226 (1967).
2. Haken, H. Cooperative phenomena in systems far from thermal equilibrium and in nonphysical systems. *Rev. Mod. Phys.* **47**, 67–121 (1975).
3. Faist, J. *et al.* Quantum cascade laser. *Science* **264**, 553–556 (1994).

4. Bennet, W. R. Jr. Hole burning effect in a He-Ne optical maser. *Phys. Rev.* **126,** 580–593 (1962).
5. Rigrod, W. W. Gain saturation and output power of optical masers. *J. Appl. Phys.* **34,** 2602–2609 (1963).
6. Osgood, R., Eppers, W. & Nichols, E. An investigation of the high-power CO laser. *IEEE J. Quant. Electron.* **QE-6,** 145–154 (1970).
7. Crowe, W. & Ahearn, W. F. Semiconductor laser amplifier. *IEEE J. Quant. Electron.* **QE-2,** 283–289 (1966).
8. Diels, J.-C. & Rudolph, W. *Ultrashort Laser Pulse Phenomena: Fundamentals, Technique, and Applications on a Femtosecond Time Scale* (Academic, San Diego, 1996).
9. Wu, Q. & Zhang, X.-C. Ultrafast electro-optic field sensor. *Appl. Phys. Lett.* **68,** 1604–1606 (1996).
10. Huber, R. *et al.* How many-particle interactions develop after ultrafast excitation of an electron–hole plasma. *Nature* **414,** 286–289 (2001).
11. Huber, R., Kaindl, R. A., Schmid, B. A. & Chemla, D. S. Broadband terahertz study of excitonic resonances in the high-density regime in $GaAs/Al_xGa_{1-x}As$ quantum wells. *Phys. Rev. B* **72,** 161314 (2005).
12. Huber, R. *et al.* Stimulated terahertz emission from intraexcitonic transitions in Cu_2O. *Phys. Rev. Lett.* **96,** 017402 (2006).
13. Koehler, R. *et al.* Terahertz semiconductor-heterostructure laser. *Nature* **417,** 156–159 (2002).
14. Walther, C., Scalari, G., Faist, J., Beere, H. & Ritchie, D. Low frequency terahertz quantum cascade laser operating from 1.6 to 1.8 THz. *Appl. Phys. Lett.* **89,** 231121 (2006).
15. Taflove, A. *Computational Electrodynamics: The Finite-Difference Time-Domain Method* (Artech House, Boston, 1995).
16. Ziolkowski, R. W., Arnold, J. M. & Gogny, D. M. Ultrafast pulse interactions with two-level atom. *Phys. Rev. A* **52,** 3082–3094 (1995).
17. Kröll, J. *et al.* Longitudinal spatial hole burning in terahertz quantum cascade lasers. *Appl. Phys. Lett.* (in the press).
18. Faist, J., Capasso, F., Sirtori, C., Sivco, D. L. & Cho, A. Y. in *Intersubband Transitions in Quantum Wells: Physics and Device Applications II* (eds Liu, H. C. & Capasso, F.) 1–83 (Academic, London, 2000).
19. Alton, J. *et al.* Buried waveguides in terahertz quantum cascade lasers based on two-dimensional plasmon modes. *Appl. Phys. Lett.* **86,** 071109 (2005).
20. Barbieri, S. *et al.* 2.9 THz quantum cascade lasers operating up to 70 K in continuous wave. *Appl. Phys. Lett.* **85,** 1674–1676 (2004).
21. Kohen, S., Williams, B. & Hu, Q. Electromagnetic modeling of terahertz quantum cascade laser waveguides and resonators. *J. Appl. Phys.* **97,** 053106 (2005).
22. Baltuska, A. *et al.* Attosecond control of electronic processes by intensive light fields. *Nature* **421,** 611–615 (2003).
23. Nuss, M. C. & Orenstein, J. in *Millimeter and Submillimeter Wave Spectroscopy of Solids* (ed. Gruener, G.) Ch. 2 (Springer, Berlin, 1998).
24. Zhang, X.-C., Hu, B. B., Darrow, J. T. & Auston, D. H. Generation of femtosecond electromagnetic pulses from semiconductor surfaces. *Appl. Phys. Lett.* **56,** 1011–1013 (1990).

Supplementary Information is linked to the online version of the paper at www.nature.com/nature.

Acknowledgements We are grateful to D. P. Kelly for comments on the presentation of the manuscript. We acknowledge financial support from the European Commission under the Integrated Project TeraNova funded by the IST directorate, and from the Austrian Science Fond (FWF) under the project Advanced Light Sources (ADLIS).

Author Information Reprints and permissions information is available at www.nature.com/reprints. Correspondence and requests for materials should be addressed to K.U. (karl.unterrainer@tuwien.ac.at).

METHODS

Spectroscopy and lasers. We use standard THz time-domain spectroscopy[8] to access the optical properties of the THz-QCL. In our specific case (Supplementary Fig. 1a), broadband THz electromagnetic pulses are generated by a gallium arsenide (GaAs) based photoconductive emitter[24] excited by 80 fs pulses at 800 nm from a Ti:sapphire mode-locked laser (pulse repetition rate is 80 MHz). The THz pulse is injected into the THz-QCL waveguide through one of the laser's facets, where it propagates along the laser cavity axis, and is re-emitted at the second facet into free space. To ensure sufficient coupling efficiency, we use a solid immersion lens approach (Supplementary Fig. 1b) to focus the THz radiation into the THz-QCL waveguide. A silicon hemisphere lens is attached directly to the laser facet. In addition, a square metallic aperture ($200 \times 200\ \mu m^2$) is placed between lens and waveguide to mask the THz transparent substrate of the laser chip.

The instantaneous electric field vector of the THz pulse is sensed using an electro-optic sampling technique based on the Pockels effect[9]. We use a 300-μm-thick gallium-phosphide (GaP) nonlinear optical crystal as electro-optic active medium. With this combination of a GaAs emitter and a GaP detector, a typical frequency spectrum between 0.5 and 3.5 THz is covered with a signal dynamic range >20 dB. Since the electro-optic detection is a coherent detection technique, only the THz radiation, which has a constant phase shift with respect to the sampling femtosecond pulse, is recorded. This phase-locked measurement is different in principle from standard transmission measurements[2–5] performed on lasers until now. Several major features emphasize the novelty of the method: (1) amplitude and phase of the amplified pulse's electric field are measured, in contrast to the standard time-averaged intensity measurements made using a probing beam; (2) broadband probing in the spectral range from 0.5 to 3.5 THz; (3) inherently high time resolution (<80 fs), which allows monitoring of the processes in the laser cavity on a subpicosecond timescale.

Response of system to THz pulse. The response of the THz medium to the injected THz pulse is obtained by examining the difference between the THz electric field transmitted through the THz-QCL, with and without bias. In order to suppress parasitic effects of scattered light and of electrical interferences in the set-up, the THz emitter and the laser are modulated at two different frequencies, ω_1 and ω_2, respectively, and the measured signal is then detected at the difference frequency $\omega_1 - \omega_2$. The spectral amplitude and phase information are obtained by standard Fourier transformation of the time domain data. The typical frequency resolution of the set-up is 30 GHz. To complement the electro-optic detection data, we use also a photo-acoustic detector (Golay cell) to record the total THz field intensity.

All the measurements are performed on AlGaAs/GaAs THz-QCL with a bound-to-continuum optical transition[19,20]. The active region of the THz-QCL consists of 90 cascades, each 125 nm long. The band structure of one period (with applied electric field) is shown in Supplementary Fig. 1c. The laser devices are processed into surface plasmon ridges 110 μm wide and 2 mm long. The laser threshold current density is $113\ A\,cm^{-2}$, the device emits single mode at 2.87 THz and operates up to a sink temperature of 70 K. All parameters refer to pulsed operation at a repetition rate of 17 kHz and a duty cycle of 15%.

The interaction of a quasi-single-cycle pulse with the optical transition in a QCL can be modelled via the interaction of an electromagnetic wave with a two-level quantum system. This approximation of a THz-QCL is adequate if we consider the lowest energy level of the injector region as the upper level of the two-level system (optical transition) and the highest energy level of the next injector region as the lower level of the two-level system (Supplementary Fig. 1c). In addition, we assume that both energy levels interact with other levels in the heterostructure via tunnelling and scattering at timescales much longer than the optical transition rate. Thus the two-level quantum system representing the optical transition can be—within a certain timescale—considered as an isolated system. We use Maxwell–Bloch equations[16] to describe the interaction of the THz pulse with this system. The results of the finite-difference time domain simulation[20] are summarized in Supplementary Fig. 2. The electric field transient forces a superposition of the wavefunctions of the ground and excited states of the two-level system and a temporal oscillating dipole is formed. The electric field emitted by this dipole is out of phase with the excitation field when the ground state population dominates, $n_a > n_b$ (Supplementary Fig. 2a). If a population inversion $n_a < n_b$ is set, the emitted electric field and the driving field are in phase (Supplementary Fig. 2b). The amplitude of the emitted field is proportional to the population difference between the ground and excited state ($n_a - n_b$) and the emission vanishes only when $n_a = n_b$. The decay of the observed oscillations is governed by the radiative and non-radiative decay of the population of the states, and by dephasing.

With respect to the measurement method, the pulse propagation effect through a gain medium of finite length has to be included in the simulation. Supplementary Fig. 2c shows the single-cycle pulse after 2 mm of propagation in the modelled gain medium. The corresponding spectral content of the pulse is shown in Supplementary Fig. 2c. The response consists of two components—a resonant main part corresponding to the eigenfrequency of the two-level system, and a broadband part that is due to the instant response of the two-level system to the driving electric field. In the latter case, the population of the states is coherently driven by the electric field of the THz pulse and a partial Rabi oscillation occurs.